Proton-Helium Elastic Scattering from 40 to 400 GeV*

E. Jenkins
University of Arizona, Tucson, Arizona 85721 USA

A. Bujak†, A. Kuznetsov, B. Morozov, V.A.Nikitin, P. Nomokonov, Y. Pilipenko, and V. Smirnov
Joint Institute for Nuclear Research, Dubna, USSR

E. Malamud, M. Miyajima≠, and R. Yamada
Fermi National Accelerator Laboratory
Batavia, Illinois 60510 USA

*This work supported in part by the U.S. Department of Energy, the U.S. National Science Foundation, and the USSR State Committee for Atomic Energy.

†Permanent Address: Institute of Nuclear Research, Warsaw, Poland.

≠Permanent Address: KEK, Japan

Report submited to the XIX International Conference on High Energy Physics, Tokyo, August, 1978.

Abstract

The elastic proton-helium differential cross sections ~~have~~ were determined for 5 different incident laboratory energies from 40 to 400 GeV in the range $0.003 < |t| < 0.52$ $(GeV/c)^2$. The differential cross section drops 4 to 5 orders of magnitude to the first dip at $|t| = 0.22$ $(GeV/c)^2$. A Glauber analysis is performed on the data. The inelastic intermediate states are found to be important. The shrinkage of the slope of the differential cross section is measured. The rate of shrinkage is twice as large as in the p-p case. Results on the real part of the elastic scattering amplitude at forward angle and at the dip structure ($|t| \approx 0.22$) are presented.

1. Introduction

Previous measurements of the elastic proton-helium differential cross sections have been made at low or intermediate energies. In particular, measurements at 1.22 GeV/c[1-4], 1.37 GeV/c[4], 1.70 - 1.75 GeV/c[5-6], and 24 GeV/c have been reported.[1] An experiment on He^4-proton elastic scattering at 1.75, 2.51, and 4.13 GeV/nucleon has been reported.[7] Measurements of e-He^4 at 1.00 GeV/c[8] and π-He^4 at 7.76 GeV/c[9] are available in the literature. These experiments all exhibit a diffraction minimum or dip in the elastic scattering. Such structure is more pronounced at higher energies.

Theoretical models to fit these diffraction minima exist.[10,11] Czyz, Lezniak, and others[12-16] have developed the Glauber multiple scattering model extensively. In multiple nucleon nucleon scattering models the first diffraction minimum arises from the interference between the single nucleon (m = 1) imaginary scattering amplitude and the multiple nucleon (m = 2, 3, 4) imaginary scattering amplitudes. At the first diffraction minimum the m = 1 and m = 2 imaginary amplitudes cancel. What remaines is a coherent sum of the single nucleon real scattering amplitude, multiple nucleon scattering ($m \geq 2$), double scattering to an intermediate inelastic state, spin nucleon effects, and possible non 2-body correlations in the nucleus. In principle the real part of the nucleon nucleon amplitude may be separated from other terms. In this experiment we have investigated elastic p-He^4 scattering with high statistical

accuracy in the energy range 40 - 400 GeV and momentum transfer squared $0.003 < |t| \leq 0.52$ $(GeV/c)^2$. The purpose of the experiment is to obtain the rate of the shrinkage of the diffraction cone and to evaluate the role of inelastic screening of the nucleons in the helium nucleus. Additionally a measurement of the real part t dependence constituted an important goal for our experiment.

In Sec. II we describe the experiment and details of analysis. At present we deal with the following set of primary energies: 45, 200, 259, 301 and 393 GeV. In Sec. III we discuss the results of the fits to the low $|t|$ region. A table with the list of parameters is given, including the slope b(s) and the real part of the amplitude. In Sec. IV we discuss the results of the fits to the whole $|t|$ region including the diffraction dip. In Sec. V we summarize our conclusions.

II. Experimental Procedure and Apparatus

The expeirmental apparatus is shown in Fig.1. The Fermilab circulating proton beam intercepted a low density, 7×10^{-7} g/cm^3, gas target. The interaction region was ≈ 10 mm. The target was viewed at near 90° by sets of totally depleted surface barrier silicon detectors with typical dimensions 5×30 mm^2. The front detectors ranged from 15 μm to 250 μm thick and the back detector was from 200 μm to 1500 μm. The silicon detectors had noise of 50 KeV and energy resolutions of 50 - 150 KeV. The detectors were 7.2 m from the target yielding a geometric angular resolution $\Delta\omega = \pm 0.7$ mrad. The resulting

kinetic energy uncertainty $\Delta T = 2T\Delta\omega/\omega$, where ω is the recoil angle with respect to 90°, was good and provided excellent separation between the elastic and inelastic reactions. Two permanently fixed stacks of detectors were used to monitor the jet-beam interaction rate. During readout of a stack the inputs to all other stacks were inhibited. Thus all channels had the same percent dead time ($\lesssim$ 3 %). Typical data rates were 1000 events per beam spill distributed over 8 detector stacks.

The $|t|$ values studied were $.003 < |t| < 0.52$ $(GeV/c)^2$, corresponding to recoil angles $6 < \omega < 96$ mrad and ranges in silicon $2 < R < 1800$ μm. In much of our t range multiple scattering of the outgoing recoil particle in the target gas was negligible to small. The multiple scattering effect was significant at our smallest $|t|$ values; in the worst case, $|t| = .003$, the multiple scattering in the target was ≈ 1 mrad. Multiple scattering mainly affects our energy resolution but does introduce small < 1 % corrections to our lowest $|t|$ cross section value.

The helium gas jet is shown in Fig.2. It has an areal density of 4×10^{-7} g/cm^2 with a jet width (RMS) ± 3 mm. Jet pulse lengths were 100 msec. and occurred twice (at two energies) during the accelerator ramp cycle. Helium was injected into a 250 ℓ buffer volume and removed by a 5000 ℓ/sec diffusion pump; 90 % of the helium was removed in this manner. The remainder was removed from the accelerator vacuum by 8 diffusion pumps spaced at 5 m intervals upstream and down stream from the target.

These pumps (4 upstream, 4 downstream) constituted a differential pumping system and reduced the helium partial pressure to $< 10^{-9}$ mm Hg beyond the final upstream, downstream points.

The detectors were calibrated with a $_{90}Th^{234}$ alpha particle source. The absolute angles determined from the elastic peak and alpha particle energy calibrations, when compared with survey measurements, show an offset difference of $\lesssim$ 0.15 mrad. We estimate our angle uncertainty at $\lesssim$ .1 mrad.

The first step in the analysis is to separate coherent He^4 recoils from H, D, T, He^3. The energies from our detector sandwiches were sorted into 256 × 256 plots of the front detector ΔE vs. the back detector $E-\Delta E$. The mass of a He^4 particle stopping in the back element is given by the empirical formula

$$m = Z^2 m_p \left[\frac{\alpha}{d_f} \left| (T_F + T_B)^\beta - T_B^\beta \right| \right]^{1/(\beta-1)} \qquad (1)$$

where $\alpha = 13.3$, $\beta = 1.73$, d_f is the thickness of the front detector in μm and $T_F(T_B)$ is the energy deposited in the front (back) detector in MeV. In Fig.3a,b we give a mass resolution plot on a logarithmic scale for $t = -0.149, -0.450$ $(GeV/c)^2$. At these t values the He^4, He^3 mass separation is excellent. The dip region, $t \approx -0.22$ $(GeV/c)^2$, where the He^4 elastic cross section has dropped 5 orders of magnitude, (the He^3 background is relatively flat) has a background systematic uncertainty far greater, as much as 50 %.

The separated He^4 recoils were expressed as momentum spectra and fitted over the range $> \pm 5\sigma$ to a formula which contained

Gaussian plus polynomial (background) terms. The number of elastic events was obtained after applying cuts at $\pm 4\sigma$ and subtracting the background determined from the fit. The background was $\lesssim 2$ % except at the lowest $|t|$, ≈ 3 %, and at the diffraction miminum ~ 50 %.

III. Small $|t|$ Region

Our results for p-He^4 elastic cross sections have been fitted in the range $0.003 < |t| < 0.07$ $(GeV/c)^2$ to the Glauber formula

$$\frac{d\sigma}{dt} = \pi |f_n + f_c|^2 \qquad (2)$$

where the Coulomb scattering amplitude takes the form

$$f_c = \frac{4\alpha\hbar}{t} G_p(t) G_{He}(t) e^{in} \qquad (3)$$

In Eq.3, α is the fine structure constant, $G_p(t) = \frac{1}{(1+|t|/0.71)^2}$ the proton electromagnetic form factor, $G_{He}(t) = [1 - (2.57t)^6]e^{11.7t}$ the He^4 electromagnetic form factor[8], $\eta = 4\alpha \ln \frac{1.06h}{R\sqrt{|t|}}$, the Coulomb phase, and $R = \sqrt{\frac{2}{3}}\langle r^2_{He}\rangle^{1/2}$ = 1.36 fm, the He^4 electromagnetic radius derived from e-He^4 scattering.

The proton and neutron density distribution are represented by

$$\psi^*\psi = \rho(\vec{r}_1, \vec{r}_2, \vec{r}_3, \vec{r}_4) = \rho_0 \cdot \prod_{i=1}^{4} e^{-\frac{r_i^2}{R^2}} \qquad (4)$$

The form for Eq.4 assumes that there are no correlations between

nucleons inside the nucleus. The elementary nucleon nucleon amplitude is written in the form

$$f_{pp} = f_{nn} = f_{pn} = \frac{\sigma_{tot}}{4\pi h}(\rho + i)e^{\frac{bt}{2}} \qquad (5)$$

with $\sigma_{tot}(mb) = 50.886 - 5.2302\ \ell n\ s_{pp} + 0.5437\ \ell n^2 s_{pp}$ an empirical fit to data of Carroll et al. The elementary nucleon nucleon amplitude is assumed to be spin, isospin independent. Such effects are not present collectively on an isospin, spin zero target nucleus such as He^4.

The Gaussian form of Eq.4 together with Eq.5 allow a closed integration over nucleon configuration space. The result is the scattering nucleon-helium amplitude, f_n, parameterized as[12]

$$f_n = \frac{i(R^2+2b)}{2\hbar}\cdot e^{-\frac{R^2 t}{16}} \sum_{m=1}^{4} K_m \binom{4}{m} (-1)^{m+1}(1-i\rho)^m \frac{1}{m}\left(\frac{\sigma_{tot}}{2\pi(R^2+2b)}\right)^m \cdot e^{\frac{(R^2+2b)t}{4m}} \qquad (6)$$

In Eq.6 we have assumed that there are no correlations between nucleons inside the nucleons and that the terms representing contributions of the inelastic intermediate states are proportional to elastic ones with enhancement coefficient K_m. Eq.6 for m = 1 yields 4 single rescattering terms; m = 2, 6 double rescattering terms; m = 3, 4 triple rescattering terms; and m = 4, one quadrupole rescattering term.

Eq.2 together with defining Eqs.3 and 6 were used to fit our results in the small $|t|$ range, $0.003 < |t| < 0.07\ (GeV/c)^2$. This equation proved inadequate to give an acceptable fit over

the full $|t|$ range $0.003 < |t| < 0.52$ $(GeV/c)^2$. The free parameters in the fit are b, the effective nucleon nucleon slope parameter, ρ, the ratio of the real part to imaginary part of the nucleon nucleon forward scattering amplitude ($t = 0$) and the overall normalization, and in another variant of the fit, the normalization plus the enhancement coefficient K_2. In Table I the results from fitting the low $|t|$ are given. In Fig.4 we plot $E_{lab} = 45$, 303 GeV data in the $|t|$ range $0.003 < |t| < 0.07$, together with the curve obtained from our fit. The ρ_{pN} values have been shown in Fig.5, the effective nucleon nucleon slope parameter has been shown in Fig.6.

In addition we have sought a model-independent description of the energy behaviour of diffraction cone of p-He^4 elastic scattering. For this purpose we used the traditional description of the differential cross section

$$\frac{d\sigma}{dt}(t) = |C \cdot e^{\frac{bt+ct^2}{2}} + f_{coulomb}|^2 \qquad (7)$$

$$b(t=t_0) = \frac{\partial}{\partial t}\left(\ell n \frac{d\sigma}{dt}\right)_{t=t_0} = b_0 + b_1 \ell n\, s \qquad (8)$$

and have found the parameters for different t-intervals. The result is given in Table II.

IV. Full Experimental $|t|$ Region

In order to analyze the data in whole available region $0.003 \lesssim |t| < 0.52$ $(GeV/c)^2$, we have employed a variant of Eq.2.

The helium nuclear density is represented as a dual Gaussian distribution

$$\Psi^*\Psi = \rho(\vec{r}_1,\vec{r}_2,\vec{r}_3,\vec{r}_4) = \rho_0 \cdot \prod_{i=1}^{4} \left(e^{-\frac{r_i^2}{R_1^2}} + C\cdot e^{-\frac{r_i^2}{R_2^2}}\right) \qquad (9)$$

The corresponding helium form-factor takes the form

$$G(q) = \frac{1}{1+D}\left(e^{-\frac{R_1^2 q^2}{4}} + D\cdot e^{-\frac{R_2^2 q^2}{4}}\right) \qquad (10)$$

The parameters D, R_1, and R_2 are determined from appropriate comparison with electron-helium elastic scattering differential cross section[8]:

$$G_{exp}(eHe) = F\cdot e^{\frac{\langle R_{He}^2\rangle^{\frac{1}{2}}}{6\cdot A}q^2}$$

$$F = G\cdot F_p \qquad (11)$$

where $G_{exp}(eHe)$ is the experimentally measured electromagnetic form factor for electron-helium scattering, F_p is the proton form factor, $e^{\frac{\langle R_{He}^2\rangle^{\frac{1}{2}}}{6\cdot A}}$ describes in an approximate way, the motion of the recoil nucleus, and A = 4 the atomic number of helium. Our fit to the electron-helium data gives the following values

$R_1 = 1.346 \pm 0.003$ fm

$R_2 = 0.678 \pm 0.014$ fm

$D = -0.033 \pm 0.003$

with $\chi^2/D.F. = 103./68.$

The Glauber amplitude has the form

$$f_n(q) = \frac{i \cdot p_0}{2\pi} \cdot e^{\frac{\langle R_{He}^2 \rangle^{\frac{1}{2}}}{4 \cdot A} q^2} \times$$

$$\times \int d^2b \; e^{i\vec{q}\cdot\vec{b}} \cdot \{1 - [1 - \frac{1}{2\pi i p} \cdot \int d^2q' \cdot e^{-i\vec{q}\cdot\vec{b}} \cdot f(q') \cdot G(q')]\}$$

$$\text{with} \quad f(q) = \frac{\sigma_{tot}}{4\sqrt{\pi}} \; P \; (\rho_0 + \rho' q^2 + i) \cdot e^{-\frac{bq^2}{2}} \qquad (12)$$

Special care has been taken in the forms for the nucleon-nucleon amplitude f(q) and the form factor G(q) in order to minimize the explicit calculation of the integrals in Eq.12. Eq.12 splits into the sum of four terms

$$f_n = f_1 + K_2 \cdot f_2 + K_3 \cdot f_3 + K_4 \cdot f_4$$

where f_i describes the i-fold rescattering amplitude of the incident proton in helium. As in the previous section the factors K_m are introduced in order to take into account in a semi-phenomenological manner the appearance of intermediate inelastic processes. We assume that inelastic intermediate states introduce enhancement factors which alter each elastic rescattering amplitude independently. The parameters K_m are the subjects for our experimental study. The most general case would be to consider K_m as complex functions of s and t (we shall not do this at present).

The fitted parameters are: N = normalisation, ρ' (see Eq.12), K_2, K_3, K_4 = enhancement coefficients of double, triple

and four-fold rescattering terms. As a constraint the values σ_{tot}^{PP} and $\frac{d}{dt} \ln|f_{PP}|^2 = b_{PP}(s, t)$ at $|t| = 0.05$ are fixed. The function $b_{PP}(s, t)$ is calculated from known data on elastic proton proton scattering. This constrains our analysis to agree with available direct information on nucleon nucleon scattering.

With these procedures we obtain good fits to our data. In Figs.7 and 8 we plot the data at $E_{Lab} = 45$ and 300 GeV in the t region $0.003 \leq |t| \leq 0.52$ $(GeV/c)^2$ together with fitted curves. The fitted parameters are listed in Table III and IV (for Table III $K_2 = K_3 = K_4 = 1$, and there is no constraint for the slope of proton proton differential cross section). The $\sigma_{tot}^{pHe}(E)$ are calculated from the fitted parameters, $\sigma_{tot}^{pHe} = \frac{\hbar}{16\pi}$ Im $f_n(t = 0)$, and are listed in Table IV. The values ρ' given in Tables III, IV are sensitive to the model parametrization; an opposite sign solution with higher χ^2 exists.

The coefficients $K_{2,3,4}$ are found to be E-dependent. In order to trace the energy dependence of inelastic screening we calculate the value

$$\Delta\sigma_{in}(E) = \sigma_{tot}^{pHe}(K_2, K_3, K_4) - \sigma_{tot}^{pHe}(K_2 = K_3 = K_4 = 1)$$

Since in the present experiment we are able to measure only relative differential cross section and σ_{tot}^{pHe} is not yet known, the value $\Delta\sigma_{in}(E)$ contains our normalisation uncertainty. In Fig.9 we plot the function $\Delta\sigma_{in}(E) - \Delta\sigma_{in}(E = 45$ GeV), in order to show the energy variation of the inelastic screening cross

section. We can again answer the question about the energy and t-dependence of the diffraction slope parameter by differentiating our fitted function

$$b_{pHe}(s, t) = \frac{d}{dt} \ln|f_n|^2 .$$

The result is shown in Fig.10.

V. Conclusions

Within the framework of the simplified Glauber model we find our low $|t|$ results yield values for the ratio of the real part to imaginary part of the forward scattering amplitude, $\rho(t=0)$, which agree well with measurements in p-p scattering as shown in Fig.5.

The effective nucleon-nucleon interaction slope parameter, b obtained from low $|t|$ analysis (see Table I and Fig.6) is significantly different from that known from proton-proton elastic scattering. This effect is also observed in proton-deuteron elastic scattering.[17] This may be attributed to the effect of inelastic scattering of nucleons in the nucleus. Indeed, we obtain a good description of the data by fixing the $b_{NN} = b_{pp}$ parameter and allowing the inelastic enhancement parameter K_2 to be free. As s increases K_2 becomes larger. This is expected since the total cross section for diffraction dissociation rises with energy.

We can obtain the diffraction cone characteristics, avoiding the Glauber formalism, simply by using the

phenomenological formula Eq.7. Fitted parameters are listed in the Table II. Parameter b_1 is again close to 1 at $t \approx 0$. The point near $t \approx 0$ may be influenced by incorrectly subtracted Coulomb scattering. The point $t \approx 0.07$ should not contain this error. There is indication that the rate of shrinkage is higher at higher $|t|$.

The whole investigated t region interval comprises the forward diffraction and Coulomb interference regions, the Glauber minimum, and the second maximum. It contains about 120 - 150 data points at each primary proton energy. The differential cross section is measured with a typical relative statistical error about 1.5 to 3 %, except the region of minimum around $|t| \sim 0.22$ $(GeV/c)^2$ where errors sometimes reach 50 %. Therefore this data set is very informative, and allows us to perform detailed Glauber analysis using equations 9 to 12. The results are presented in Table III and IV.

The fits show a ρ' term, the linear dependent term in $\rho(t) = \rho_0 + \rho'|t|$, of ≈ 4.0 independent of energy. At the minimum of cross section the contribution of this term becomes large and the real part of the amplitude turns out to be of the order of 100 % of imaginary one. Unfortunately at present state of analysis we feel that ρ' may be greatly changed by another choice of nucleon-nucleon amplitude parametrization. So more work remains to be done to be certain about the value for $\rho(t \neq 0)$.

The important feature of the present analysis is the

search for inelastic intermediate states in the helium nucleus. The fits show that enhancement coefficients K_2, K_3, K_4 are very important. They have different values. Surprisingly K_4 is high. The fourfold rescattering is increased some 60 times with respect to the elastic one due to inelastic intermediate processes. In order to understand this result let us consider all possible rescattering graphs in p-He^4 collisions as illustrated in Fig.11. There is only one graph representing double rescattering (Fig.11(1)). According to our definition the enhancement due to inelastic processes comes as a factor $\sqrt{k}$ at each vertex, so the double rescattering amplitude has a factor

$$K_2 = 1 + k \tag{13}$$

There are two graphs representing the triple rescattering (Fig.11(2a, b)). It is seen from the graphs 2a and 2b that there are two types of vertices in this case and that they may have different factors which are denoted as $\sqrt{k}$ and $\sqrt{k'}$, so the triple rescattering amplitude has an enhancement factor

$$K_3 = 1 + k\sqrt{k'} + 2k \tag{14}$$

Similar consideration for four-fold rescattering (Fig.11 (3a-d)) leads us to formula

$$K_4 = 1 + kk' + 3k + 2k\sqrt{k'} + k^2 \tag{15}$$

The parameters K_2, K_3, and K_4 are fitted independently.

From Eqs. 13 and 14 one can find values for k and k' and from Eq.15 predict the value for K_4. The predicted value for K_4 is shown in Table IV together with fitted one. They are in close agreement with each other, which gives support for this model of inelastic screening in proton helium interaction.

Another characteristic of the model is the behaviour of the pHe total cross section. It can be easily calculated as $\sigma_{tot} \sim \text{Im } f_n(0)$. The calculated values are listed in the Table IV. In Fig.9 we show the function $\delta = \Delta\sigma_{in}(E) - \Delta\sigma_{in}(45\ \text{GeV})$ which visualizes the role of inelastic screening. $\delta_{pHe} = (2.37 \pm 0.18) \ln \frac{s}{s_0}$. This is to be compared with corresponding value for pd scattering: $\delta_{pd} = (0.52 \pm 0.1) \ln s/s_0$. Levin and Strickmann[11] have estimated that the inelastic term in pHe is much more predominant than in pd scattering, namely $\sigma_{in}(\text{pHe}) \approx 10 \cdot \sigma_{in}(\text{pd})$. We find this prediction qualitatively true.

In Fig.10 we show the rate of shrinkage of diffraction cone of pHe elastic scattering, making use of the derivative of the Glauber differential cross section with all parameters fitted (and shown in Table IV). The result obtained in this manner is in agreement with previously obtained parameters $b^{pHe}(E)$, $b_1^{pHe}(t)$ (Fig.6 and Table III). Here we again observe the rate of shrinkage of pHe cone twice as large as for pp-scattering. At higher $|t|$ the rate of shrinkage is higher:

$$b_1^{pHe}(|t| = 0.01) = 0.74 \pm 0.1$$
$$b_1^{pHe}(|t| = 0.1) = 1.0 \pm 0.1$$
$$b_1^{pHe}(|t| = 0.13) = 1.35 \pm 0.1$$

REFERENCES

1. J. Berthot et al., International Conference on High Energy Physics and Nuclear Structure, Santa Fe, (1975). 2nd International Conference on Elementary Particles, Aix-en-Provence, (1973).
2. E. T. Boschitz et al., Phys. Rev. C6, 457 (1972); E. T. Boschitz et al., Phys. Rev. Lett. 20, 1116 (1968).
3. J. Fair et al., Nucl. Phys. A262, 413 (1976).
4. S. L. Verbeck et al., Phys. Lett. 59B, 339 (1975).
5. H. Palevsky et al., Phys. Rev. Lett. 32, 839 (1974); E. Aslanides et al., Sixth International Conference on High Energy Physics and Nuclear Structure, Santa Fe, N.M., (1975).
7. V. Avdeichikov, Journal of Nucl. Phys. (Sov.) 27, 710 (1978).
8. R. F. Frosch et al., Phys. Rev. 160, 874 (1967). J. S. McCarthy et al., Phys. Rev. 15C, 1396 (1977).
9. T. Ekelöf et al., Nucl. Phys. B35, 493 (1971).
10. E. M. Levin and M. I. Strikman, Leningrad Nuclear Physics Institute, Report 203 (1975).
11. R. Bassel and Wilkin, Phys. Rev. 174, 1179 (1968).
12. W. Czyz and L. Lesniak, Phys. Lett. 24B, 227 (1967).
13. W. Czyz and L. Lesniak, Phys. Lett. 25B, 319 (1967).
14. W. Czyz and L. Maximon, Phys. Lett. 27B, 354 (1968).
15. W. Czyz et al., Nucl. Phys. B19, 125 (1970).
16. H. Lesniak and L. Lesniak, Nucl. Phys. B36, 221 (1972).
17. D. Gross et al., Phys. Rev. Lett. (1978).
18. M. Ikeda, Phys. Rev. C 6, 1608 (1972).

TABLE AND FIGURE CAPTIONS

Table I

	1st variant			2nd variant			
E_{Lab} [GeV]	b_{pN}	ρ_{pN}	χ^2/D.F.	b_{pp}(fixed)	ρ_{pp}(fixed)	K_2	χ^2/D.F.
44.9	10.57 ± .16	-0.152 ± 0.037	55./54	10.72	-0.150	0.998 ± 0.011	55./55
45.5	10.74 ± .18	-0.134 ± 0.040	42./47	10.73	-0.149	1.017 ± 0.012	42./48
199.6	12.13 ± .13	-0.048 ± 0.025	49./52	11.53	-0.040	1.102 ± 0.008	52./53
259.3	12.40 ± .14	-0.040 ± 0.035	40./42	11.67	-0.019	1.132 ± 0.010	37./43
301.0	12.57 ± .12	-0.013 ± 0.026	44./49	11.76	-0.008	1.139 ± 0.008	43./50
393.3	12.75 ± .16	0.000 ± 0.040	48./44	11.90	+0.012	1.136 ± 0.010	53./45

$$b_{pN} = (6.27 \pm 0.44) + (0.98 \pm 0.08) \times \ln s$$
$$\rho_{pN} = (-0.045 \pm 0.010) + (0.067 \pm 0.017) \times \ln s$$

Table II

$$b\,(t=t_0) = b_0 + b_1 \times \ln s$$

Interval of (t)	Average $\langle t \rangle = t_0$	b_0	b_1	χ^2/D.F.
0.003 - 0.07	0.03	25.3 ± 0.5	1.25 ± 0.06	1.4/4
0.04 - 0.11	0.07	29.1 ± 0.5	0.94 ± 0.07	3.2/4
0.08 - 0.16	0.12	32.0 ± 0.8	1.31 ± 0.11	11.1/4

Table III

$\rho(t) = \rho_0 + \rho' |t|$

Energy [GeV]	b_{pN}	ρ_0 (fixed)	ρ'	χ^2/points
44.9	11.13 ± 0.03	-0.150	-0.19 ± 0.04	332./136
45.5	11.14 ± 0.03	-0.149	-0.16 ± 0.03	280./115
199.6	12.42 ± 0.03	-0.040	-0.22 ± 0.03	634./140
259.3	12.35 ± 0.03	-0.019	-0.16 ± 0.03	390./122
301.0	12.64 ± 0.03	-0.008	-0.22 ± 0.04	259./134
393.3	12.76 ± 0.03	+0.012	+0.22 ± 0.05	382./129

Table IV

Energy [GeV]	Input values $b_{pN}(t=0.05)$	$\frac{\partial}{\partial t}\ln(\frac{d\sigma}{dt})_{pp}(t=0.05)$	Fitted values ρ_0	ρ'	K_2	K_3	K_4	χ^2/points	Calculated values σ_{tot}^{pHe}	$K_4=f(K_2,K_3)$
44.9	10.90		-0.150	-3.87±0.31	1.38±0.02	6.76±0.18	70.0±1.3	202./136	132.05±0.33	76.38
45.5	10.90		-0.149	-4.08±0.32	1.39±0.02	6.73±0.22	69.2±1.7	141./115	132.09±0.38	75.49
199.6	11.44		-0.040	-3.91±0.15	1.57±0.04	7.85±0.47	70.5±5.1	192./140	129.98±0.20	70.72
259.3	11.57		-0.019	-4.08±0.16	1.54±0.03	7.19±0.35	62.3±3.8	154./122	130.99±0.18	61.26
301.0	11.65		-0.008	-3.66±0.15	1.64±0.03	8.51±0.31	74.2±3.2	185./134	130.53±0.17	76.45
393.3	11.81		+0.012	+3.64±0.15	1.48±0.04	6.54±0.45	53.9±4.6	153./129	133.29±0.25	55.53

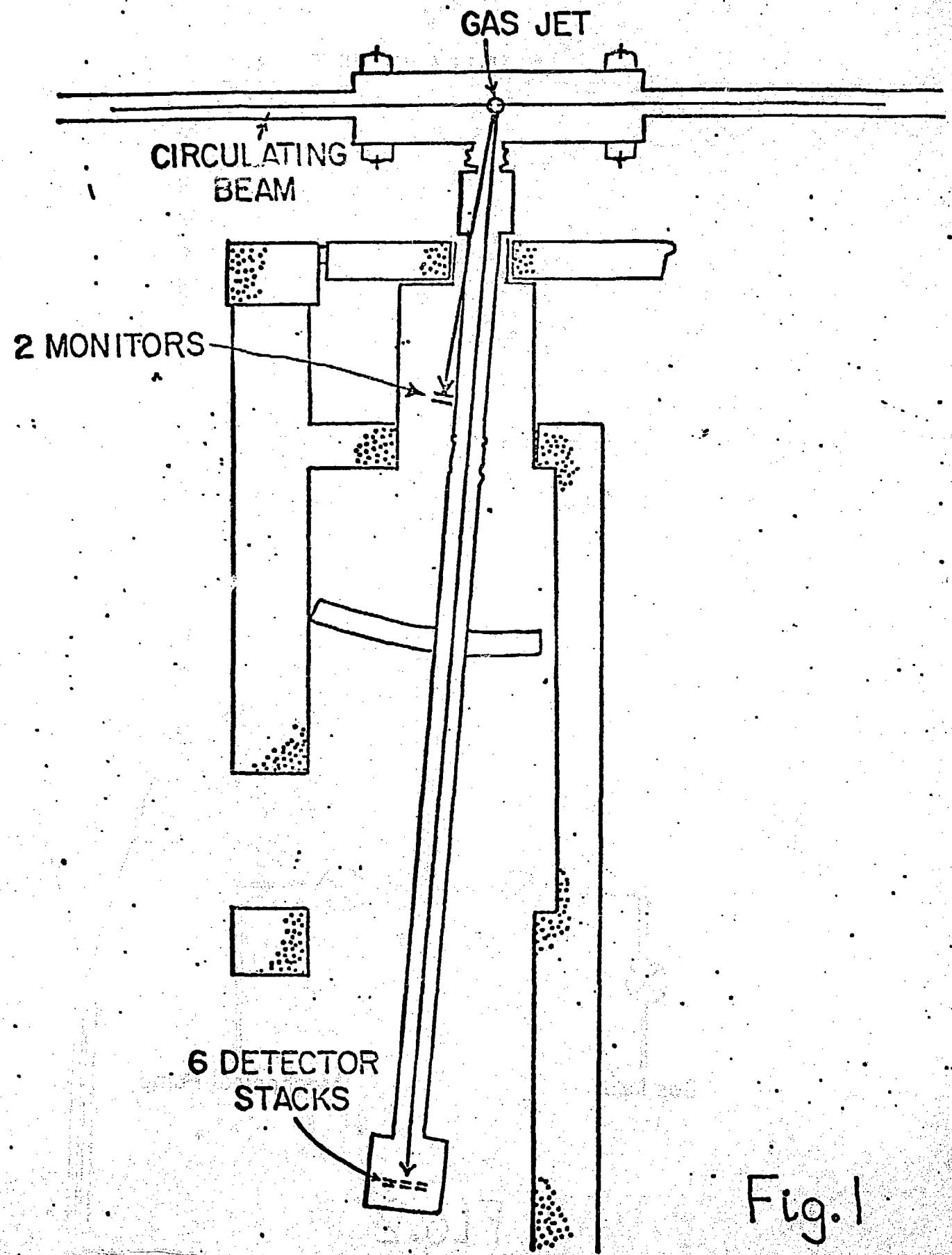

Fig. 1

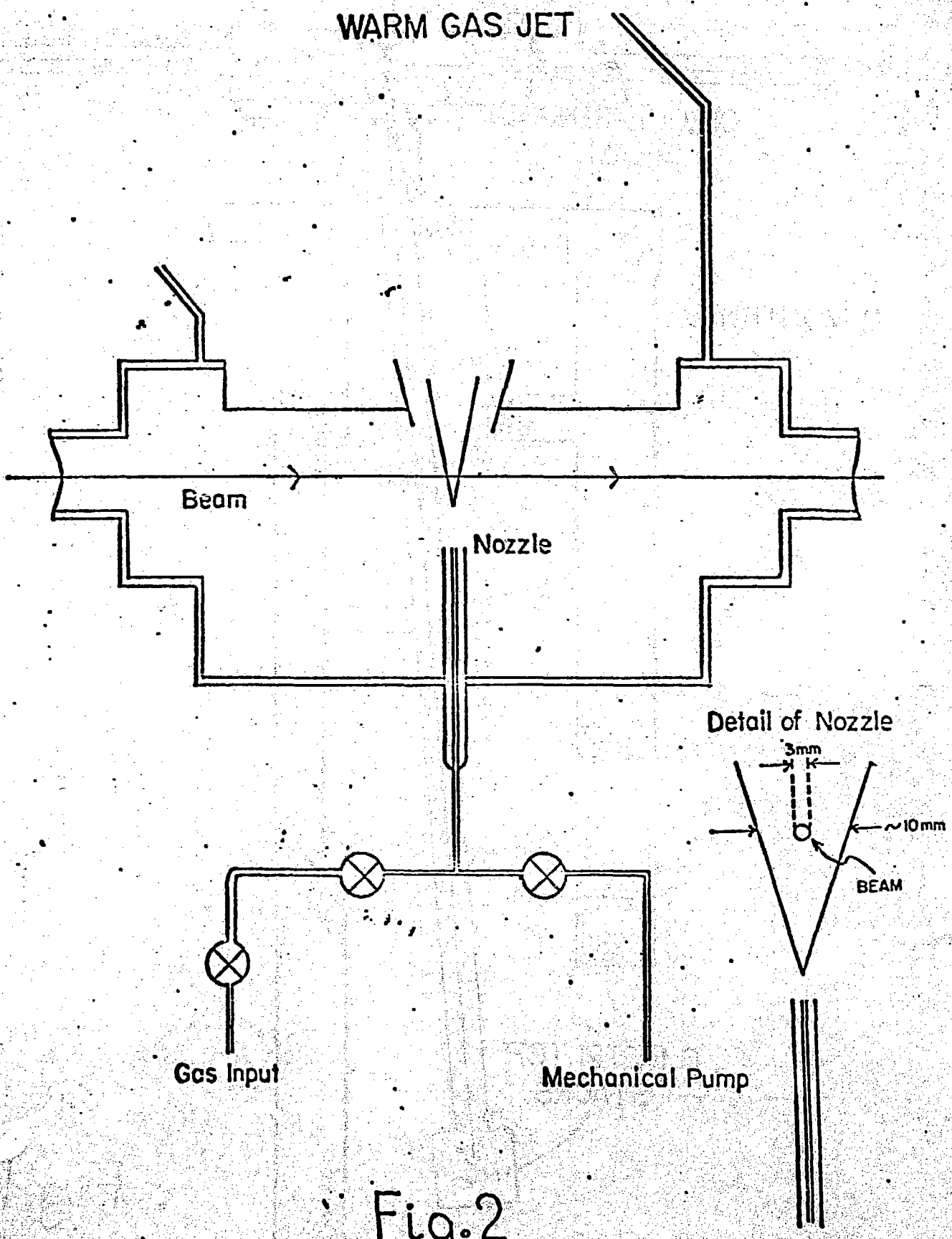
WARM GAS JET
Beam
Nozzle
Detail of Nozzle
3mm
~10mm
BEAM
Gas Input
Mechanical Pump

Fig. 2

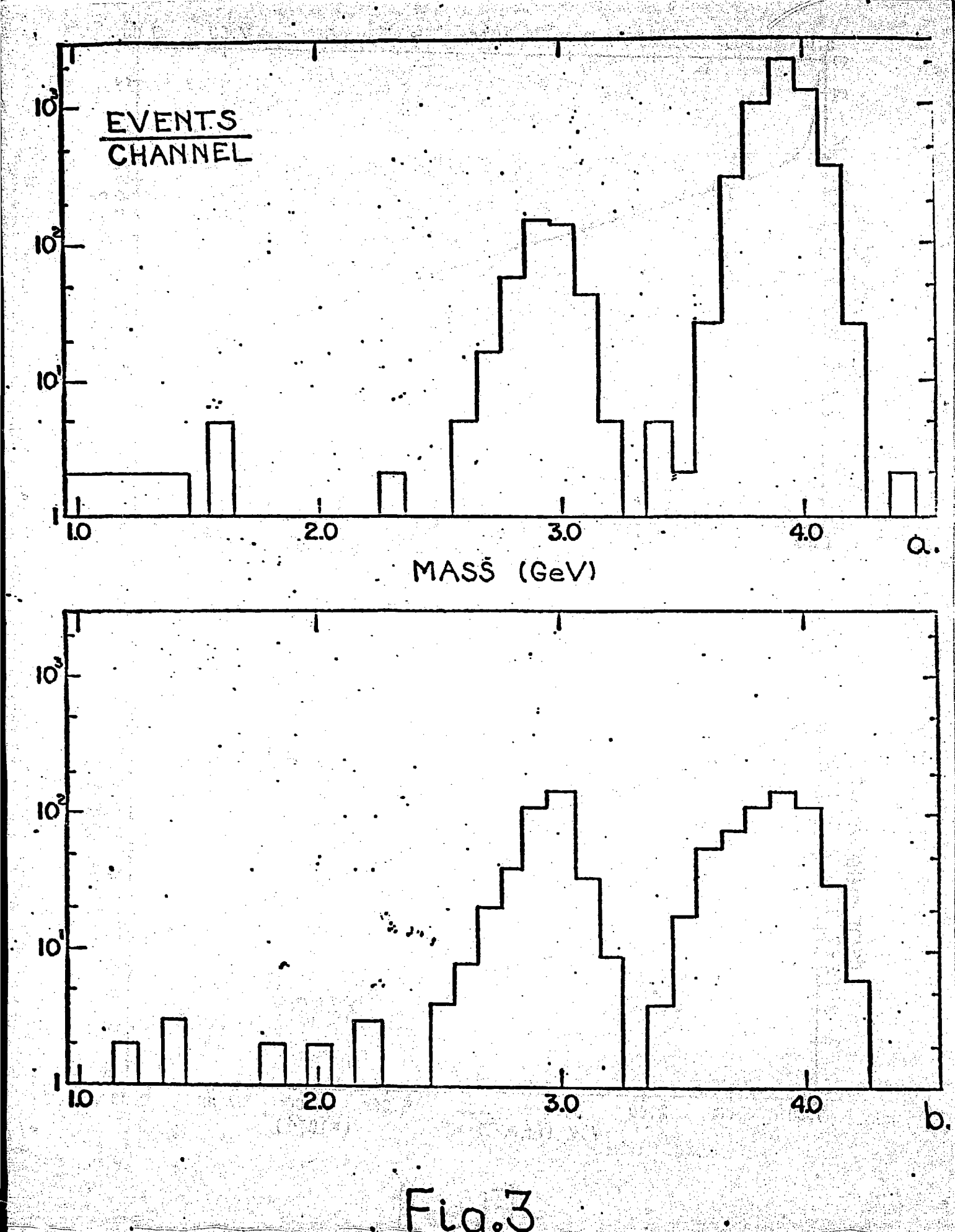
EVENTS
CHANNEL
10³
10²
10¹
1
1.0
2.0
3.0
4.0
a.
MASS (GeV)
10³
10²
10¹
1
1.0
2.0
3.0
4.0
b.

Fig.3

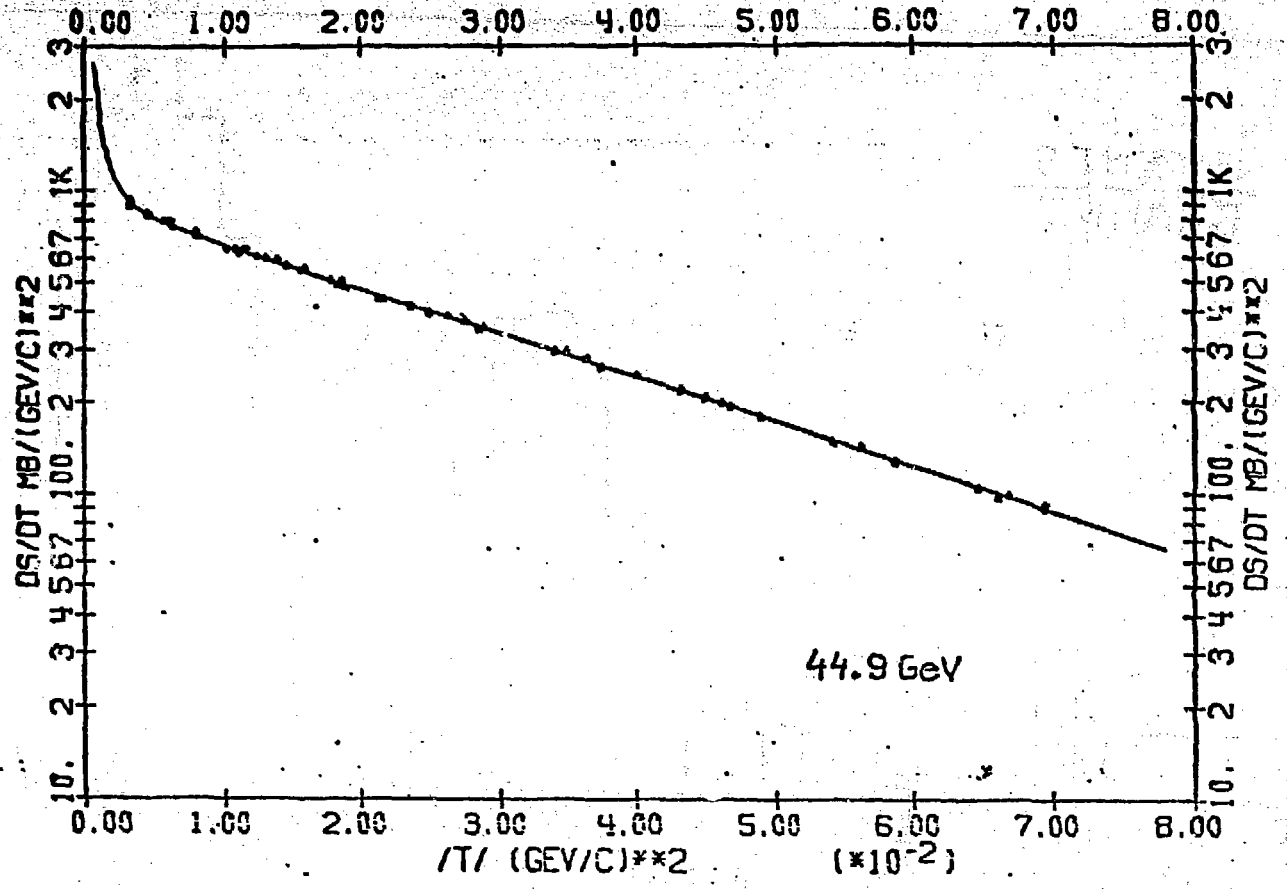
0.00 1.00 2.00 3.00 4.00 5.00 6.00 7.00 8.00
DS/DT MB/(GEV/C)**2
10. 100. 1K
44.9 GeV
/T/ (GEV/C)**2 (*10^-2)

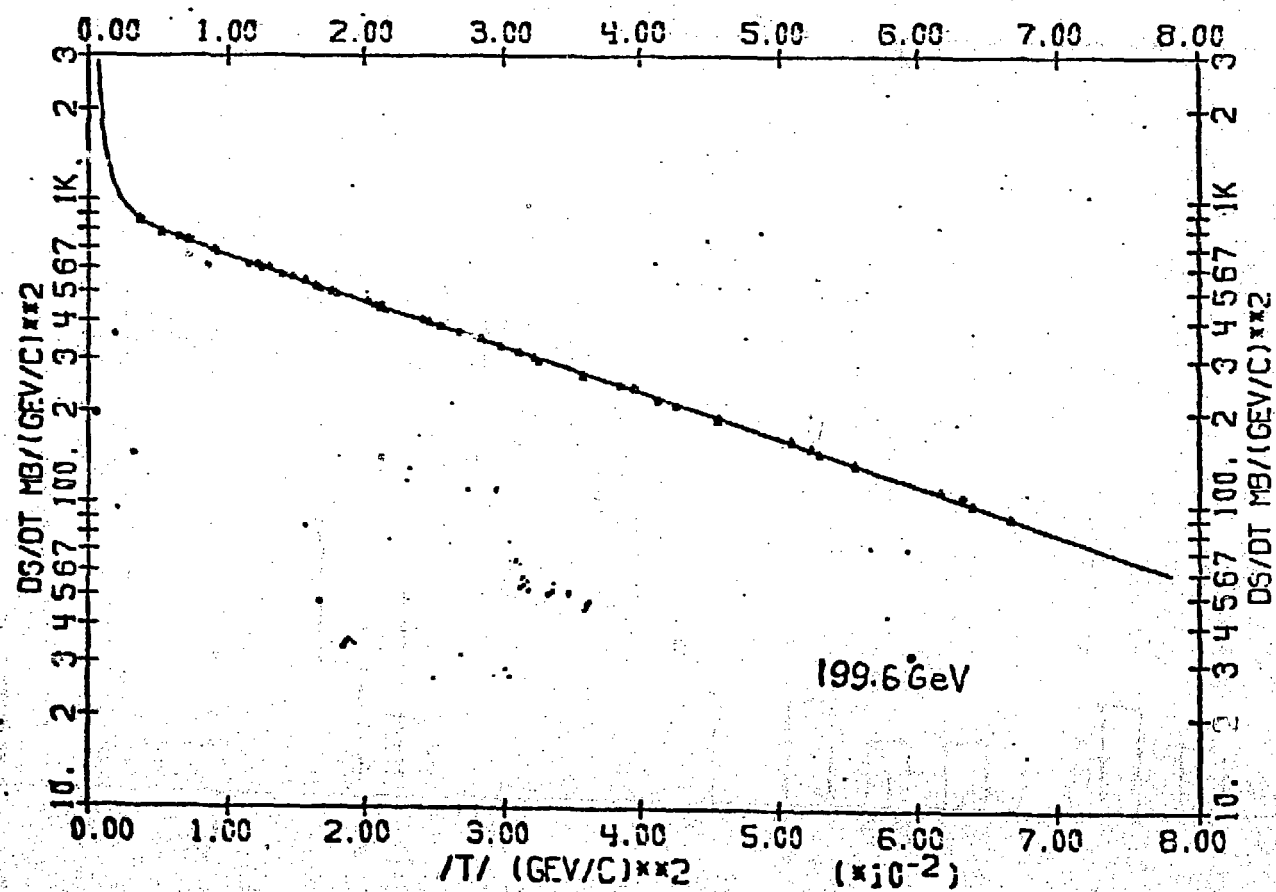
0.00 1.00 2.00 3.00 4.00 5.00 6.00 7.00 8.00
DS/DT MB/(GEV/C)**2
10. 100. 1K
199.6 GeV
/T/ (GEV/C)**2 (*10^-2)

Fig. 4

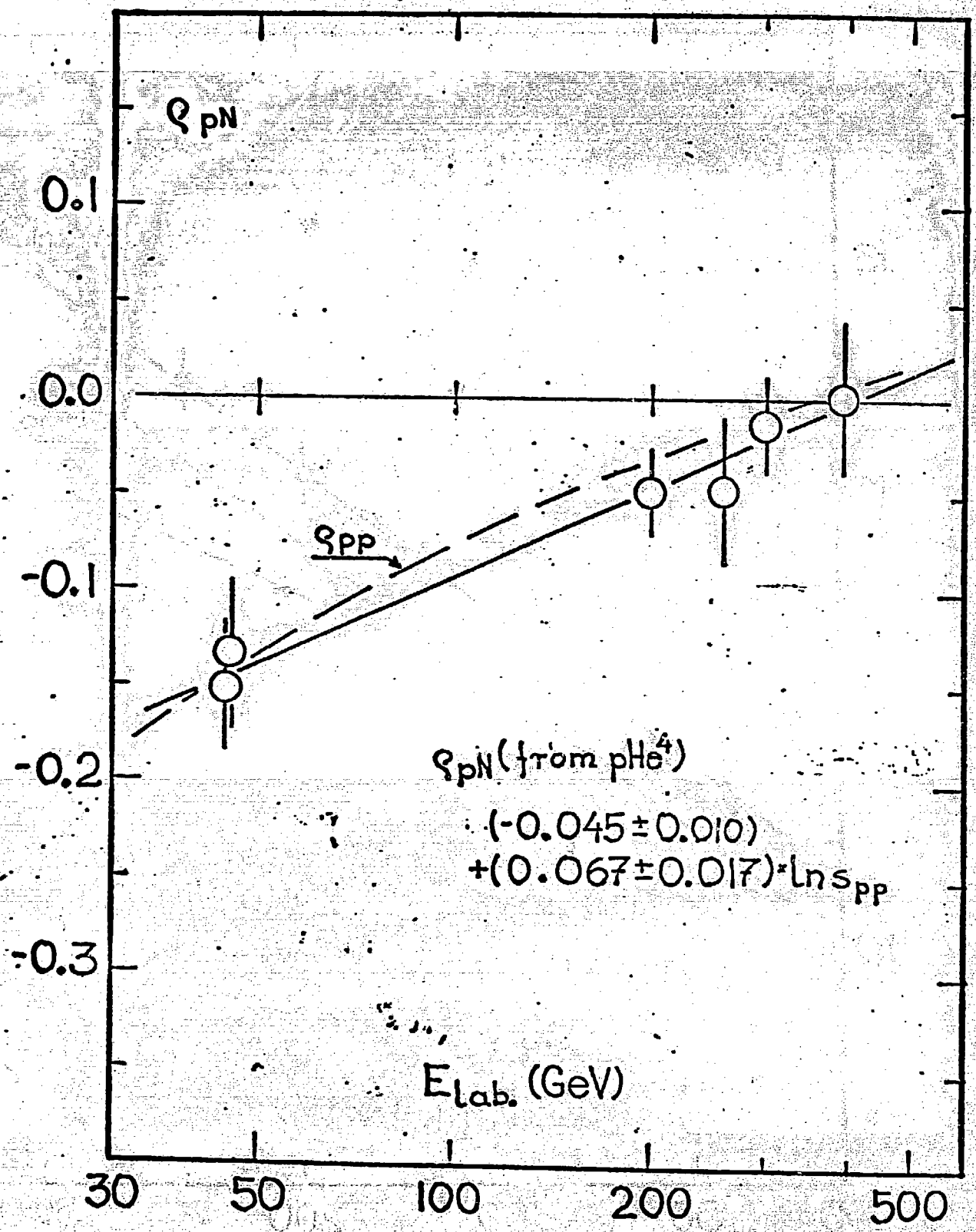
ρpN
0.1
0.0
-0.1
-0.2
-0.3
ρpp
ρpN(from pHe⁴)
(-0.045±0.010)
+(0.067±0.017)·ln s_pp
E_lab. (GeV)
30
50
100
200
500

Fig.5

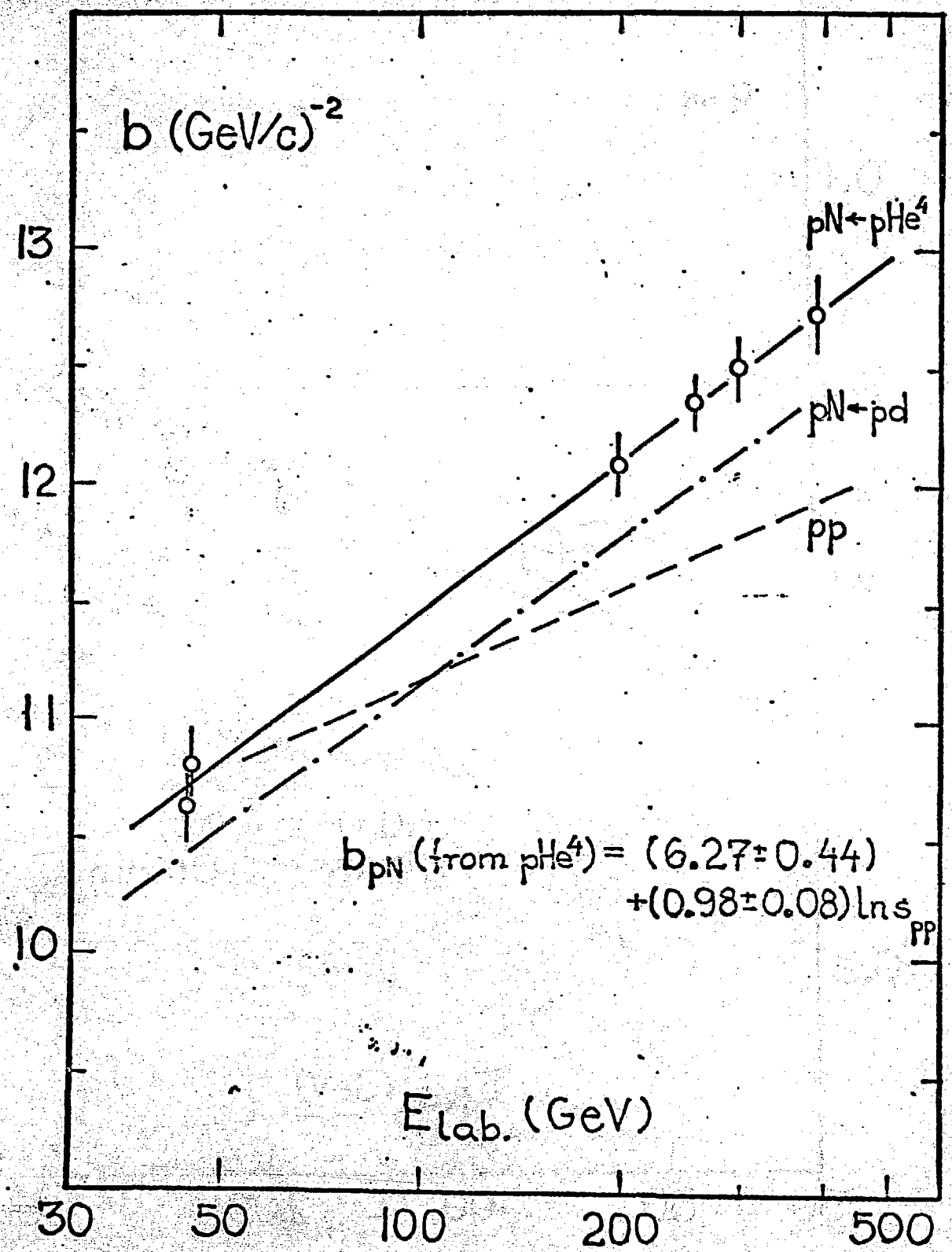
b (GeV/c)$^{-2}$
13
12
11
10
pN←pHe^4
pN←pd
pp
b_{pN} (from pHe^4) = (6.27±0.44)
+(0.98±0.08) ln s_{pp}
$E_{lab.}$ (GeV)
30
50
100
200
500

Fig. 6

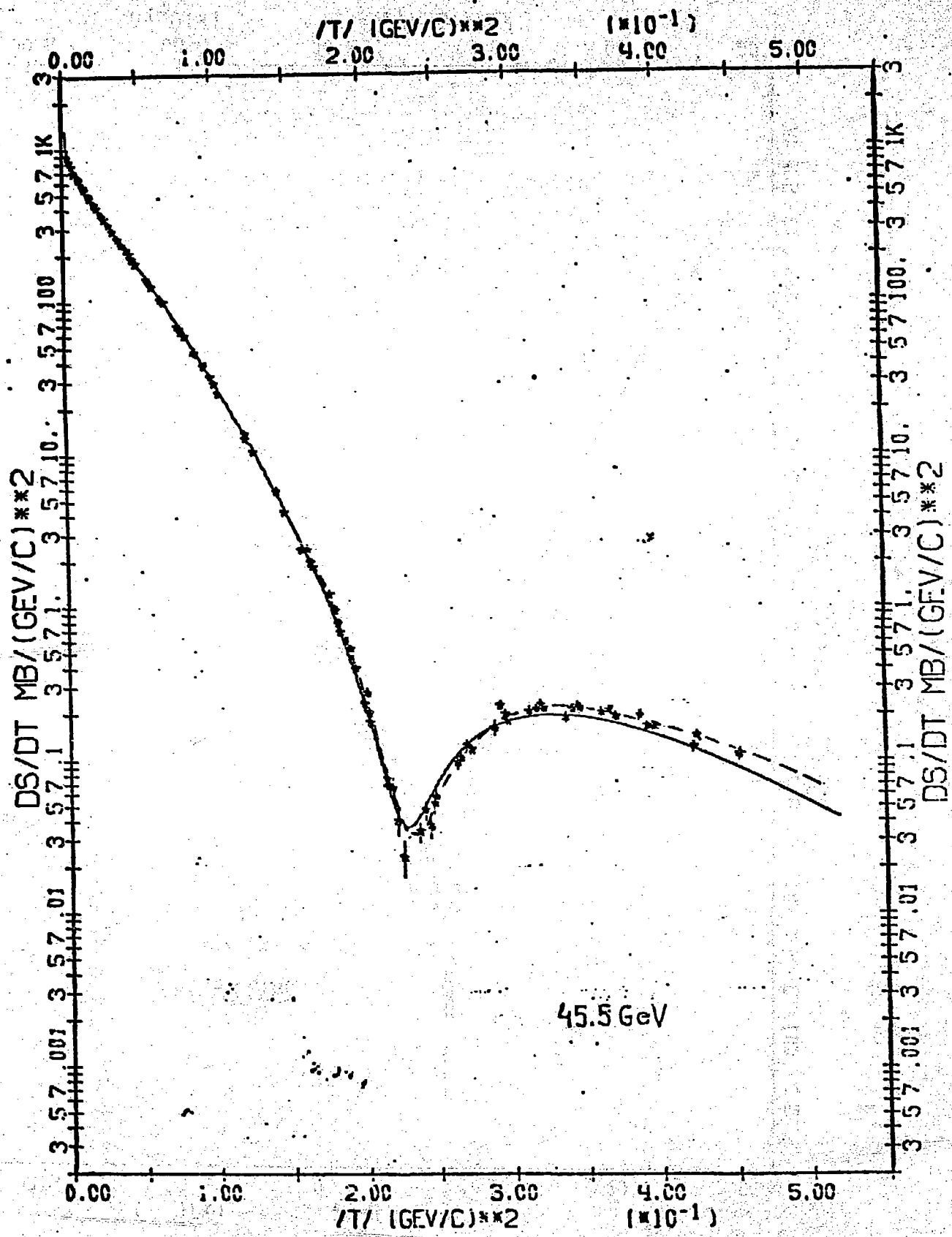

Fig. 7

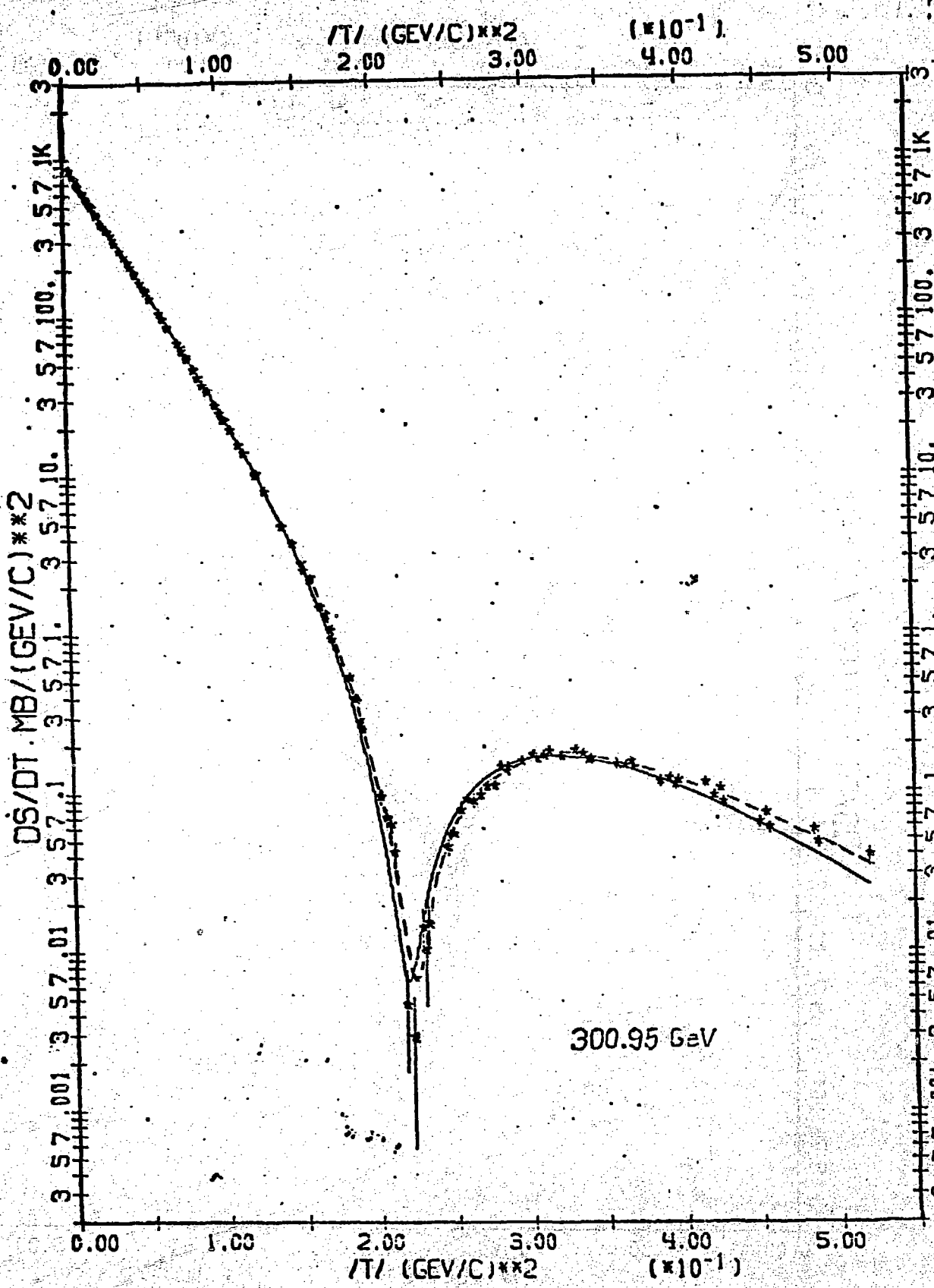

Fig.8

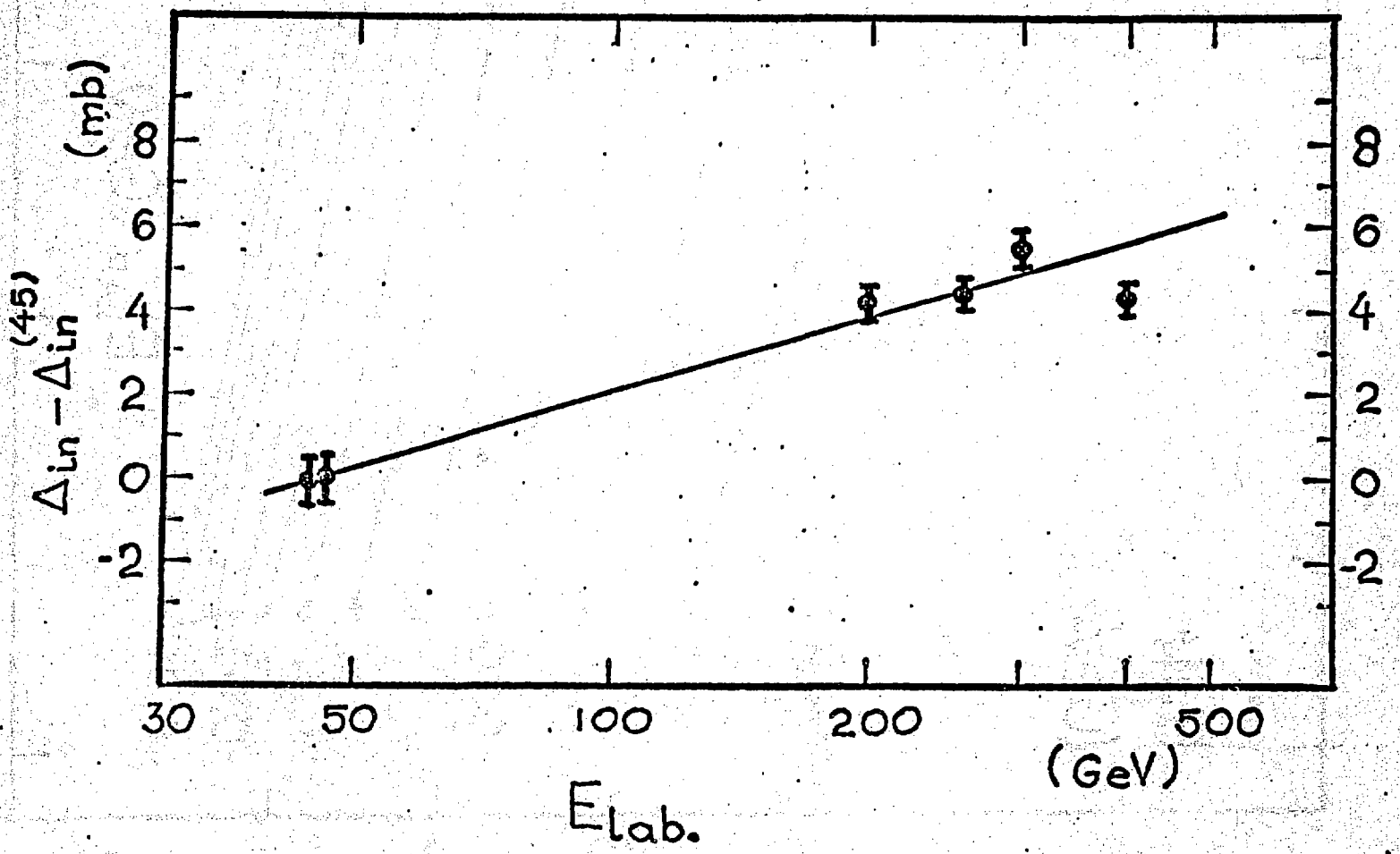

Fig. 9

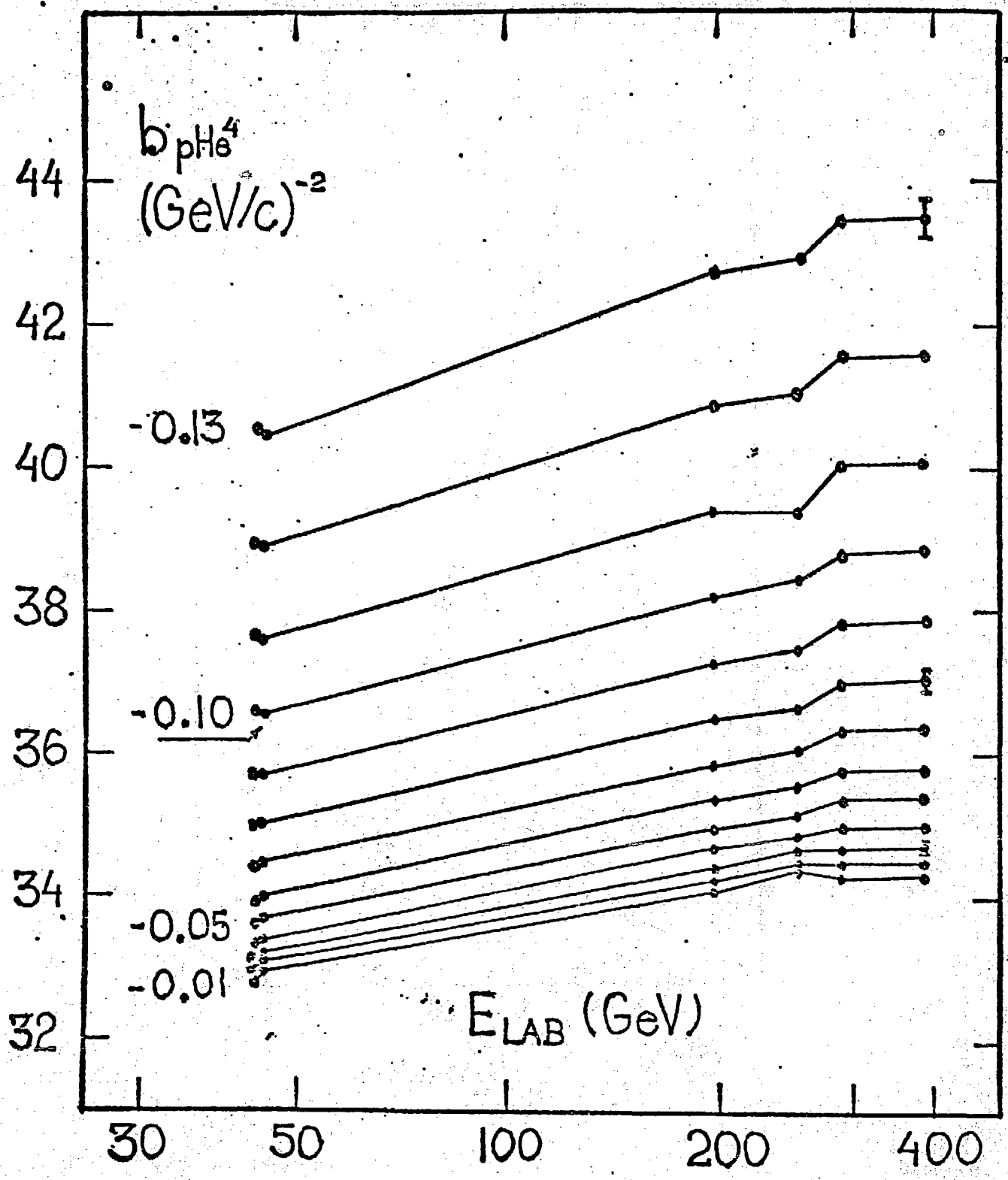
b_{pHe^4}
$(GeV/c)^{-2}$
44
42
40
38
36
34
32
-0.13
-0.10
-0.05
-0.01
E_{LAB} (GeV)
30
50
100
200
400

Fig. 10

1. 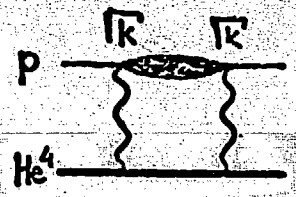

$= g^2 k$ (definition)

2.a). 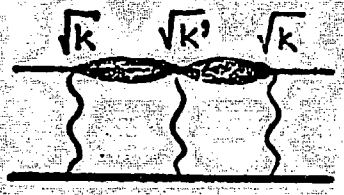

$= g^3 k\sqrt{k'}$

b). 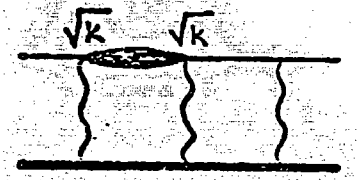

$= 2g^3 k$

3.a). 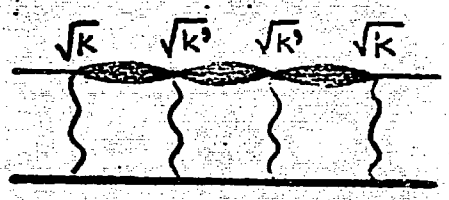

$= g^4 k k'$

b). 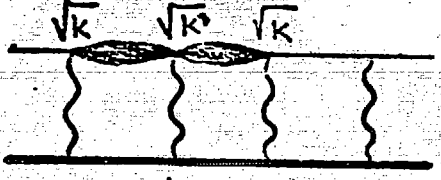

$= 2g^4 k\sqrt{k'}$

c). 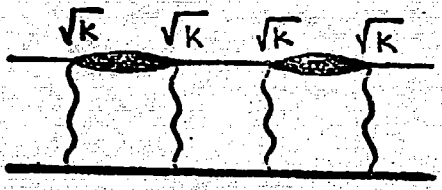

$= g^4 k^2$

d). 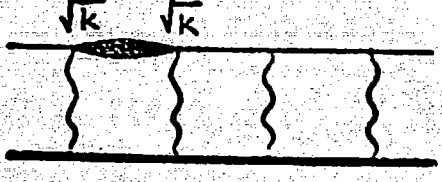

$= 3g^4 k$

Fig. 11